

Provided for non-commercial research and education use.  
Not for reproduction, distribution or commercial use.



This article appeared in a journal published by Elsevier. The attached copy is furnished to the author for internal non-commercial research and education use, including for instruction at the authors institution and sharing with colleagues.

Other uses, including reproduction and distribution, or selling or licensing copies, or posting to personal, institutional or third party websites are prohibited.

In most cases authors are permitted to post their version of the article (e.g. in Word or Tex form) to their personal website or institutional repository. Authors requiring further information regarding Elsevier's archiving and manuscript policies are encouraged to visit:

<http://www.elsevier.com/copyright>



Contents lists available at ScienceDirect

Biochimica et Biophysica Acta

journal homepage: [www.elsevier.com/locate/bbamem](http://www.elsevier.com/locate/bbamem)

## Efficacy of external tetraethylammonium block of the KcsA potassium channel: Molecular and Brownian dynamics studies

David Bisset, Shin-Ho Chung\*

Research School of Biological Sciences, Australian National University, Australia

### ARTICLE INFO

#### Article history:

Received 31 March 2008

Received in revised form 22 May 2008

Accepted 22 May 2008

Available online 3 June 2008

#### Keywords:

Potassium ion channel

Tetraethylammonium

TEA

KcsA

Brownian dynamics

Conductance

Ion permeation

### ABSTRACT

Blockade of the KcsA potassium channel by externally applied tetraethylammonium is investigated using molecular dynamics calculations and Brownian dynamics simulations. In KcsA, the aromatic rings of four tyrosine residues located just external to the selectivity filter create an attractive energy well or a binding cage for a tetraethylammonium molecule. We first investigate the effects of re-orienting the four tyrosine residues such that the centers of the aromatic rings face the tetraethylammonium molecule directly. Then, we systematically move the residues inward in both orientations so that the radius of the binding cage formed by them becomes smaller. For each configuration, we construct a one-dimensional free energy profile by bringing in a tetraethylammonium molecule from the external reservoir toward the selectivity filter. The free energy profile is then converted to a one-dimensional potential energy profile, taking the available space between the tyrosine residues and the tetraethylammonium molecule into account. Incorporating this potential energy profile into the Brownian dynamics algorithm, we determine the conductance properties of the channel under various conditions, construct the current-tetraethylammonium-concentration curve and compare it with the experimentally determined inhibitory constant  $k_i$  for externally applied tetraethylammonium. We show that the experimentally determined binding affinity for externally applied tetraethylammonium can be replicated when each of the four tyrosine residues is moved inward by about 0.7 Å, irrespective of orientation of their aromatic rings.

© 2008 Elsevier B.V. All rights reserved.

### 1. Introduction

Nearly all potassium channels are blocked by externally applied tetraethylammonium (TEA). The sensitivity to TEA, however, differs in different types of  $K^+$  channels. Some channels, such as the *Shaker*  $K^+$  channel, require concentrations of tens of millimolar of TEA to attenuate the current by a half of the control value [1–4], whereas other channels, such as the KcsA  $K^+$  channel, require only a few millimolar or less TEA to achieve the same degree of current attenuation [5]. The binding affinity of TEA can be drastically enhanced in *Shaker* by replacing the threonine residue at position 449 with the tyrosine or phenylalanine residue [5,6] or reduced in KcsA by replacing tyrosine at position 82 with cysteine or threonine [1]. Thus, at least in KcsA and the mutant *Shaker*, TEA in the external face of the channel is attracted by a binding cage formed by four aromatic rings of the tyrosine residues. Although the details remain to be fully elucidated, the attractive electrostatic [7] or hydration forces [8,9] between the benzene ring and the charged TEA molecule create an energy well and the conduction pathway for  $K^+$  ions is effectively occluded once a molecule is bound to the binding pocket.

In other potassium channels, the mechanisms underlying extracellular blockade by TEA may be quite different. In the Kv2.1 channel, which is a slowly inactivating delayed rectifier responsible for repolarization of the action potential, the current block by external TEA hinges on several factors. For example, TEA is ineffective in blocking  $Na^+$  currents flowing across this channel in the absence of  $K^+$  [2]. The substitution of the tyrosine residues at position 380 (corresponding to position 449 in *Shaker*) with cysteine residues has a relatively small effect on TEA block; this mutation shifts the inhibitory constant from 3 to 9 mM [10]. Thus, the stabilization of TEA in the external vestibule appears to be influenced by, among other factors, the conformation of the vestibule, the electrostatic environment near the binding pocket, and the occupancy state of the selectivity filter [11]. It is possible that, in the course of a prolonged activation of the channel, TEA efficacy undergoes dynamic changes, as do the conformations of the external vestibule [12,13] and the selectivity filter [14].

Here we demonstrate that Brownian dynamics (BD) simulations, together with the one-dimensional free energy profile computed using molecular dynamics (MD), can reveal further insights into the action of externally applied TEA on the permeation dynamics. A novel Brownian dynamics simulation algorithm is implemented that comprises two potential energy profiles; the standard profile is seen by the potassium and chloride ions in the simulation assembly and the

\* Corresponding author. Fax: +61 2 6 125 0739.

E-mail address: [shin-ho.chung@anu.edu.au](mailto:shin-ho.chung@anu.edu.au) (S.-H. Chung).

MD-derived profile is applied to the TEA molecules. We first compute one-dimensional free energy profiles under different orientations of the tyrosine side-chains. Such profiles show shallow attractive wells just outside the selectivity filter, extending about 6 Å in the direction normal to the membrane [8,9]. The one-dimensional free energy profile, computed from molecular dynamics calculations, is then converted into a one-dimensional potential energy profile and incorporated into the BD algorithm. In this algorithm, the motion of TEA is influenced by the random and frictional forces, and the external electrostatic field, in addition to the MD-derived free energy profile. This energy profile, invisible to other charged particles in the reservoirs and channel, is in turn modulated by the locations of resident  $K^+$  ions in the selectivity filter. The BD simulations are run for a period long enough to study the effects of TEA in the simulation assembly on the conductance properties of the KcsA  $K^+$  channel. The ability to run simulations over a period long enough to determine statistically consistent estimates of the current flow across ion channels is a distinct advantage of BD over molecular dynamics.

With this modification of the BD algorithm, we carry out simulations of the KcsA potassium channel with KCl ions and TEA molecules both present. We first show that the free energy profile constructed from the crystallographic structure of the KcsA [15] gives an attractive potential well extending about 6 Å from the external end of the selectivity filter. The depth of the well is 4.5 kcal/mol or 7.6 kT, which corresponds closely to the value reported by Crouzy et al. [8]. The current-TEA-concentration curve obtained from BD simulations incorporating this free energy profile gives the inhibitory constant that is far greater than the value reported experimentally [1]. We then systematically reduce the radius of the binding cage formed by the four aromatic rings and construct the free energy profiles at various configurations. The depth of the energy well increases steadily as the radius of the binding cage is decreased. When the tyrosine residues are brought inward by 0.4 and 0.9 Å, making the distance between the center of the pore and the carbon- $\gamma$  of TYR82 7.7 and 7.2 Å, respectively, the inhibitory constants of TEA applied at the external side of the channel become 5 and 0.6 mM. These  $k_i$  values are close to those reported for the T449Y *Shaker* mutant [6] and the KcsA channel [5]. We show that the blocking and unblocking of TEA obey a first-order Markovian process. With a 4 mM TEA concentration, the channel stays blocked for the mean duration of 300 ns. The number of water molecules surrounding TEA in the binding cage, we show, is systematically reduced as its radius decreases.

## 2. Methods

### 2.1. Channel models

The model channel we used for BD simulations is based on the crystal structure of Doyle et al. [15] with the radius of the pore expanded at the internal end of the channel to 5 Å, using a cylindrical repulsive potential in molecular dynamics. As described previously [16], the selectivity filter is also expanded slightly such that the minimum radius is 1.4 Å. We assign the full charge of  $-e$  to ASP80 and  $+e$  to ARG64 located at the extracellular aspect of the channel, whereas partial charges of  $-0.5e$  and  $+0.5e$  are assigned to the ionizable pair GLU118 and ARG117 guarding the intracellular gate. One unpaired arginine residue (ARG27), and the two pairs of ionizable residues (GLU51-LYS52 and GLU71-LYS89) are kept neutral, for the reasons detailed in Chung et al. [17]. This model replicates the experimental data, such as the observed current-voltage-concentration profiles [16].

### 2.2. Molecular dynamics calculations

The system used for MD simulations was based on an initial set of coordinates from a previous simulation of TEA interacting with KcsA, made available to us by Crouzy and his colleagues [8]. The TEA

molecule is in its lowest energy, symmetrical planar conformation, and is initially docked in the deepest KcsA blocking position. No constraints are applied that would prevent the TEA from changing its conformation. The KcsA tetramer is embedded in a DPPC bilayer surrounded by approximately 150 mM solutions of KCl. All ionizable residues are in their standard states except that GLU71 is protonated. The system contains 14  $K^+$  and 23  $Cl^-$ , making it electrically neutral. Binding sites S1–S4 of the selectivity filter contain water- $K^+$ -water- $K^+$ , which are unconstrained but they are very stable in this configuration. Simulations are carried out with CHARMM [18] v32b1 and the PARAM27 force field [19], with periodic boundary conditions and particle mesh Ewald electrostatics. The TIP3 model is used for water, and partial charges on the atoms of the TEA molecule are assigned as in Crouzy et al. [8]. To keep the system position stable, harmonic constraints with coefficient 10.0 kcal/mol Å<sup>2</sup> (16.9 kT/Å<sup>2</sup>) are applied to the outer helices of the protein, and also to the nonhydrogen atoms of the lipid bilayer in the  $z$ -direction only (normal to the plane of the bilayer). The selectivity filter and its surrounding loops and pore helices are unconstrained.

Profiles of potential of mean force (PMF) are calculated, under two different orientations of the aromatic rings of TYR82 ('edge-on' and 'en face' orientations), using umbrella sampling [20] and the weighted histogram analysis method (WHAM) [21]. A harmonic biasing potential of 14.8 kcal/mol Å<sup>2</sup> (25 kT/Å<sup>2</sup>) is applied between the centers of mass of TEA and the backbone atoms of the selectivity filter (THR75–TYR78). Successive runs of (usually) 100 ps of data are stored for each series of biasing positions separated in  $z$  by 0.5 Å. For longer runs of data lasting up to 2 ns, the individual runs are joined end-to-end before all positions are processed together with WHAM.

In the edge-on configuration, the aromatic rings are tilted relative to the central axis by various degrees, whereas in the *en face* configuration, they are positioned such that their centers face the edge of a TEA molecule. The positions and orientations of the TYR82 side-chain rings are maintained with the CHARMM MMFP planar constraint during *en face* PMF calculations. Average positions of the TYR82 C $\gamma$  atoms are determined after unmodified runs, and planar constraints are set up passing through those positions with the planar normal facing C $\gamma$  from the diagonally opposite protein subunit. For the runs that test the effects of bringing the tyrosine rings closer together, the C $\gamma$  positions are all moved toward the center of the pore by equal distances. We use the MMFP force constant of 10.0 kcal/mol Å<sup>2</sup> for most cases.

For the edge-on cases, where TYR82 is moved inward but the orientation of the side-chain ring is not predetermined, the movement is accomplished by constraining the positions of the TYR82 backbone N, C and C $\alpha$  atoms and the side-chain C $\beta$ . Similarly to the *en face* cases, the average positions of the specified atoms were determined from unmodified runs, and constraints were set after the atoms had been moved toward the center of the pore by equal distances.

### 2.3. Brownian dynamics simulations

Brownian dynamics offers one of the simplest methods for following the trajectories of interacting ions in a fluid. To carry out BD simulations, we first place in three-dimensional space all the atoms forming the KcsA channel at the center of the assembly, and assign the charge on each atom. Then, a large cylindrical reservoir of 30-Å radius with a fixed number of  $K^+$  and  $Cl^-$  ions is attached at each end of the channel to mimic the extracellular or intracellular space. Ions are initially assigned random positions with a specified mean concentration and Boltzmann-distributed velocities within cylindrical reservoirs. The membrane potential is imposed by applying a uniform electric field across the channel. This procedure is equivalent to placing a pair of large plates far away from the channel and applying a potential difference between them. Since the space between the voltage plates is filled with electrolyte solution, each reservoir is in isopotential. The average potential anywhere in the reservoir is

identical to the applied potential at the voltage plate on that side, and the potential drop occurs almost entirely across the channel.

The algorithm for performing BD simulations is conceptually simple. The ions follow the equation of motion known as the Langevin equation, a stochastic version of Newton's equation. At every time-step, the forces acting on each ion are calculated and the Langevin equation is used to determine where it will move in the next time-step. The calculation is repeated for each ion in the assembly, and the new distribution of the positions of all ions at time  $t + \Delta t$  is assigned. A multiple time-step algorithm is used, where a time-step of  $\Delta t = 100$  fs is employed in the reservoirs and 2 fs in the channel where the forces change more rapidly. If an ion is inside the short time-step region at the beginning of a 100-fs period, then that ion is simulated by 50 short steps while the other ions in the long-time regions are frozen to maintain the synchronicity. By repeating this process many billions of times, usually for simulation periods lasting up to 1 ms, we can trace the movement of each ion in space during a simulation period, and count how many ions have crossed from one side of the channel to the other. The algorithm for carrying BD simulations is described in details elsewhere [22–24].

What ultimately determines the movement of ions across the channel is the force acting on them. Thus, all components of the force have to be calculated correctly to deduce the current flowing across the channel using computer simulations. Among the sources that contribute to the electric field in the channel are (i) the membrane potential, (ii) charged residues in the protein and on the protein wall, (iii) ions everywhere in the simulation assembly, and (iv) charges induced on the protein wall by those ions. All the components of the force, except (iii), are calculated by solving Poisson's equation without imposing any symmetries on either the channel shape or the position of ions. As the equation cannot be solved using analytically for complicated protein–water boundaries formed by biological ion channels, we resort to iterative numerical techniques, according to the procedures detailed previously [25]. The last two sources interact dynamically. As an ion moves from one position to another, the pattern of induced charges changes, and induced surface charges in turn impede the motion of the ion as it approaches the protein–water boundary. We compute each of these components at each discrete time-step, either using Poisson's equation or Coulomb's law, and add them up to obtain the total force acting on each ion. In addition, to prevent two ions from coming too close to each other, a repulsive short-range potential, varying as  $1/r^9$ , is included. This steeply rising potential imitates the repulsive force produced when the electron shells of two ions begin to overlap [26]. If two ions at any time step are positioned within  $3/4$  of the sum of the ionic radii, then their trajectories are traced backward in time until such a distance is exceeded. The procedure is implemented to ensure that the forces at the next time-step do not become so large to make the ions to leave the simulation system, due to numerical problems arising from two finite time-steps.

The electrostatic forces  $F_\lambda$  acting upon the ions are calculated by solving Poisson's equation using a boundary element method [27]. Two free parameters needed to solve Poisson's equation are the dielectric constant of the protein forming the channel  $\epsilon_p$  and of water inside the pore  $\epsilon_w$ . The dielectric constant  $\epsilon$  is a dimensionless number that tells us by what factor the force between two charged particles is reduced relative to that in vacuum. In bulk water, water molecules orient around and shield charged particles such that electrostatic interaction between the charged particles is reduced by a factor of approximately  $1/80$ . This shielding is likely to be less in a channel than in bulk water, since the rotational motion of water molecules is constrained in narrow pores and thus they are unable to fully coordinate around an ion. Thus, one should use a lower value of  $\epsilon_w$  in the channel when solving Poisson's equation, but exactly what value should be used is unknown. Assigning the appropriate value of the dielectric constant of protein  $\epsilon_p$  is also nontrivial. Proteins are quite heterogeneous, exhibiting large variations in polarizability depending on whether we are dealing with the interior

or exterior of protein [28]. Molecular dynamics studies of globular proteins reveal that the effective  $\epsilon_p$  for the whole protein varies between 10 and 40 [29,30]. However, when only the interior region of the protein consisting of the back-bone and uncharged residue is considered,  $\epsilon_p$  varies from 2 to 4. In ion channels, water is embedded in protein, rather than protein embedded in water. Thus, assigning a fixed  $\epsilon_p$  value to a channel protein in continuum electrostatic calculations is problematic, as noted by Burykin et al. [31,32]. In one earlier MD study on trypsin [33], the effective dielectric constant in the interior of the protein is estimated to be as high as 10. As these constants are difficult to measure experimentally or deduce theoretically, Ng et al. [34] solve the inverse problem to determine the most appropriate values to be used in BD simulations. Using the MthK channel, they used various values of  $\epsilon_p$  and  $\epsilon_w$  and compared the current-voltage relationships obtained from BD simulations with the experimental curve. The best agreement is obtained when  $\epsilon_p$  and  $\epsilon_w$  are assumed to be, respectively, 2 and 60. They showed that the precise value of  $\epsilon_p$  used for BD simulations has negligible effects on the magnitude of currents flowing across the MthK channel. We adopt  $\epsilon_p = 2$  and  $\epsilon_w = 60$  for the present study. Because the boundary element method used to solve Poisson's equation does not permit ions to cross dielectric boundaries, a uniform dielectric constant of 60 is employed throughout channel and reservoir water. The change from reservoir ( $\epsilon_w = 80$ ) to channel water ( $\epsilon_w = 60$ ) is instead represented by a Born energy barrier of 0.6 kT. This barrier is introduced as a smooth switching function at the channel entrance [24].

Since calculating the electric forces at every step in the simulation is very time consuming, we store pre-calculated electric fields and potentials due to one and two ion configurations in a system of lookup tables and interpolate values for the given ion positions from these during the simulation [23]. To prevent charged particles from leaving the system, a hard-wall potential is activated when they are within one ionic radius of the reservoir boundaries. To ensure that the desired intracellular and extracellular ion concentrations are maintained throughout the simulation, a stochastic boundary is applied. When an ion crosses the channel, an ion of the same species is transplanted so as to maintain the original concentrations on both sides of the membrane. Im et al. [35] have used a more complicated technique of maintaining concentration in reservoirs, but as shown by Corry et al. [36], these two methods give virtually the same current-voltage-concentration profiles. They also demonstrate that both methods give the expected binomial distribution of ions near the channel entrance. These results follow from the fact that the time it takes to attain a stationary distribution in the reservoirs is much smaller than the time it takes for a single ion to cross the ion channel.

A temperature of 298 K is assumed throughout. The diffusion coefficients for  $K^+$  used in the selectivity filter and elsewhere inside the channel pore are 0.1 and 0.5 of the bulk value, respectively [37]. The diffusion coefficient is related to the friction coefficient  $\mu$  by the Einstein relation.

#### 2.4. Tetraethylammonium in the BD algorithm

The shape of a TEA molecule is an oblate spheroid, generated by the revolution of an ellipse, with the major and minor axes equal to 4.6 and 2.3 Å. The molecule can take two different conformations in the solution. In one conformer, the end carbon atoms (CB) bend downward, forming a pyramidal shape, whereas in the other conformation the central nitrogen atom, the adjacent carbon atoms (CA), and the end carbon atoms all form a planar configuration [9]. For MD calculations, we use the latter conformer, and for BD simulations, we approximate its shape as a sphere with the radius of 2.3 Å. The results of BD simulations obtained with two different radii (2.3 and 3.4 Å) are virtually identical. The molecular weight and diffusion coefficients used for the spherical TEA model are, respectively, 130.25 and  $0.87 \times 10^{-9} \text{ m}^2\text{s}^{-1}$  [38].

Each one-dimensional free energy profile (PMF) obtained from MD calculations is converted to a potential energy profile for TEA in the BD

program. To do this, we first fit to the averaged profile an analytical expression, which is the sum of three simple algebraic functions. The parameters featuring in the algebraic functions are adjusted to a least-square fitting using the Lavenberg–Marquardt method [39]. Then this fitted free energy profile is converted to the one-dimensional potential energy profile required for BD, taking the effective cross-sectional area at each  $z$  position into account. The energy well at the TEA binding site becomes about 3 kT deeper when the free energy profile is converted to the potential energy profile. The relationship between the one-dimensional free energy and the one-dimensional potential energy is given in Hoyles et al. [40]. A BD reference potential is independently calculated by bringing a TEA toward the binding site along the axis of the channel in the full BD system, but excluding short-range repulsive forces. The BD reference potential is then subtracted from the potential profile to avoid double counting of potentials already included from the molecular dynamics free energy profile. Then, the one-dimensional potential profile is matched to this BD reference potential at its outer end, where the TEA is surrounded by extracellular solution. Both the PMF and the BD reference potential are calculated with two  $K^+$  ions in the selectivity filter. The positions of the two  $K^+$  ions in the selectivity filter are allowed to vary to minimize the total energy. These two positions range from  $z = 9.55$  to  $9.71$  Å, and from  $z = 16.47$  to  $16.66$  Å. Any change in  $K^+$  configuration during the main BD simulations is accounted for as all ion-ion interactions are calculated at every time-step.

The position of the center of mass of the selectivity filter, which is taken as the origin of the  $z$ -axis for MD calculations, is at  $z = 15.1$  Å in our coordinate system (where  $z = 0$  is taken to be at the midpoint between the two ends of the channel). The coordinate system of the one-dimensional potential energy profile derived from the PMF is offset accordingly. During the main BD simulations, all the forces encountered by ions in the simulation assembly are applied to TEA molecules in the reservoir. In addition, a TEA molecule encounters the one-dimensional potential derived from the PMF when it is in the range  $24.1 \leq z \leq 31.1$  Å.

We employ, when needed to maintain lower concentrations of TEA in the external reservoir, the grand canonical Monte Carlo method [35]. The effective volume of each reservoir in our simulation system is  $8.7 \times 10^{-26}$  m<sup>3</sup>. Since placing one molecule in the reservoir will bring its concentration to ~20 mM, we make use of this method to maintain a low TEA concentration, rather than increasing the size of the reservoirs. The technical details of implementing the grand canonical Monte Carlo method are given in Corry et al. [36]. The TEA concentration observed in the reservoir deviates appreciably from that stipulated in the input of the grand canonical Monte Carlo method. Thus, for each concentration, we count the average number of TEA molecule in the exterior reservoir and use this value for the actual concentration.

### 3. Results

#### 3.1. Free energy profiles from MD calculations

The aromatic rings of the four tyrosine residues at position 82 of KcsA are able to rotate and assume various orientations with respect to the central axis. In Fig. 1, we illustrate two possible configurations of the aromatic rings. The starting coordinates used for this study, depicted in Fig. 1A, show that the side-chains of TYR82 are tilted and rotated by various degrees. We refer to this configuration, after Ahern et al. [7], an 'edge-on' orientation. The figure shows a TEA molecule at the center of the binding cage. Ahern et al. [7] provide evidence to support that, to establish optimum  $\pi$ -cation interactions between the tyrosine residues and a TEA molecule, the aromatic ring needs to be oriented such that its center would point to the edge of a TEA molecule. Such a configuration, referred to as an 'en face' orientation, is illustrated in Fig. 1B. We mold the side-chains of TYR82 by

changing the orientations and the positions of the aromatic rings. We define the radius of the TEA binding pocket as the mean distance between the central axis of the pore and the center of the carbon- $\gamma$  that is attached to the carbon- $\beta$  of TYR82. This measure allows consistent comparison of the changes made to *en face* and edge-on sizes of the binding cage.

The radius of the binding pocket obtained from the coordinates of the crystal structure [15] is, using our definition, 8.8 Å. It is reduced to 8.3 Å when the structure is embedded in the lipid bilayer and then fully equilibrated. In the starting configuration, the TYR82 side-chain is turned about 25° away from exactly edge-on. The plane of the

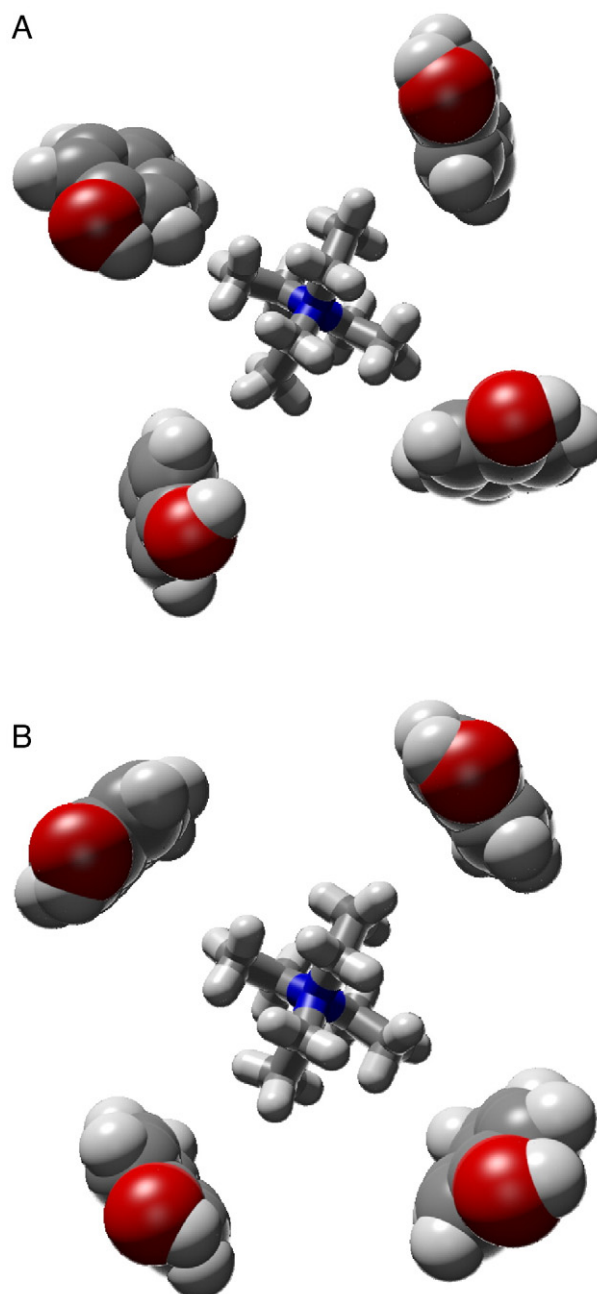


**Fig. 1.** Orientation of the aromatic rings of four tyrosine at position 82 of the KcsA potassium channel. These four side-chains constitute the binding cage for a TEA molecule, shown in the center of each figure. (A) In the crystal structure, the aromatic rings are tilted by various degrees relative to a TEA molecule at the center of the binding cage. Thus, the edges of the molecule face the edges of the tyrosine side-chains. This configuration of the aromatic rings is referred to as an 'edge-on' configuration. (B) The orientation of the aromatic rings is tilted such that their centers are facing the edge of a TEA molecule. This configuration is referred to as an 'en face' orientation.

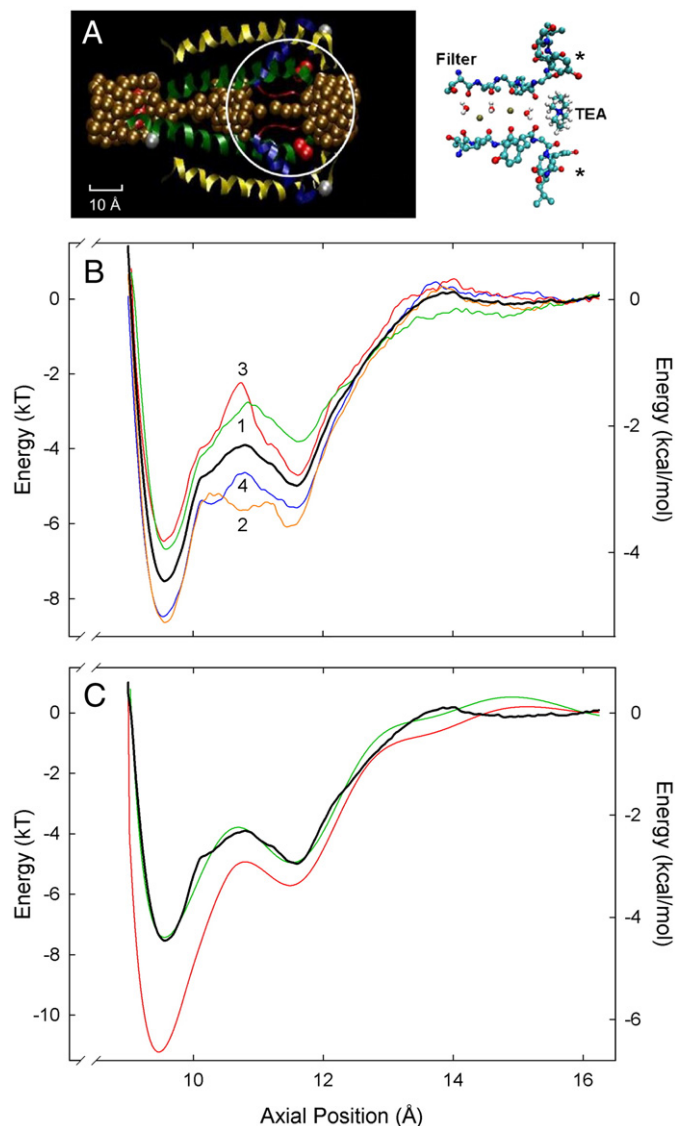


**Fig. 2.** The potential of mean force encountered by a TEA molecule. (A) Two of the four subunits of the full experimentally determined KcsA protein are represented as ribbons. Water molecules are shown in gold. The circled region of the protein, containing the selectivity filter, is enlarged on the right-hand side and shown in a stick- and-ball model, together with three water molecules and 2  $K^+$  ions (gold). Two of the four tyrosine residues forming the TEA binding cage are indicated in asterisks. (B) The profiles of potential of mean force (PMF) are calculated from the crystal structure of KcsA using molecular dynamics. Four such profiles are calculated during the successive simulation periods of 500 ps, indicated by the number accompanying each graph. The x-axis refers to the distance of the TEA from the center of the mass of the selectivity filter. (C) An analytical function (green) is first fitted to the average of four profiles (solid line). Then, the one-dimensional PMF profile is converted to a one-dimensional potential energy profile, which is then incorporated into the BD algorithm after adding a short-range force.

aromatic ring is not vertical but leans inward from the vertical plane, also by about  $25^\circ$ . The centers of the side-chains of the four tyrosine residues form a square, with each side with a length of 11.8 Å [8]. Using this configuration, we construct a set of free energy profiles using MD calculations.

Fig. 2A shows the structure of KcsA that is hydrated with water molecules (shown as gold spheres). An enlarged section of the channel with a TEA molecule in the binding pocket is illustrated on the right-hand side. With 2 $K^+$  ions in the selectivity filter, the structure is first equilibrated for 200ps. Then, a set of 4 free energy profiles are calculated using the umbrella sampling method during the successive simulation periods of 500 ps (0.2–0.7, 0.7–1.2, 1.2–1.7, and 1.7–2.2 ns).

These profiles, labelled 1, 2, 3, and 4 in Fig. 2B, are plotted against the distance from the center of mass of the selectivity filter. If  $z = 0$  is taken to be midpoint between the two ends of the channel, the center of mass of the backbone of the residues 75–78 (i.e., TVGY) is  $z = 15.1$  Å. The well starts at about  $z = 15$  Å and reaches its deepest point at  $z = 9.3$  Å (or 24.4 Å from the midpoint between the two ends of the channel), but its magnitude fluctuates from 6.6 to 8.5 kT. The Boltzmann average of the four free energy profiles is shown in solid line. The averaged profile is first fitted with an analytical function, composed of 3 simple algebraic functions (Fig. 2C, green), which is then converted to a one-dimensional potential energy (Fig. 2C, red), and grafted onto the BD algorithm. The depth of the well, after this conversion, increases to 11.1 kT. In this novel BD algorithm, the motion of TEA is influenced by the electrostatic, random, and frictional forces, as well as the attractive force arising from its interaction with four tyrosine residues. This free energy profile, invisible to other charged particles in the simulation assembly, is in turn modulated by the locations of resident  $K^+$  ions in the selectivity filter. Further details of the BD algorithm that incorporates the potential energy profile of TEA are given in Hoyles et al. [40].

### 3.2. Blockade of currents by TEA

Using the profile with the (free energy) well depth of approximately 7.5 kT at  $z = 24.4$  Å (or  $z = 9.3$  Å from the center of mass of the selectivity filter), we construct the current-TEA-concentration profiles at three different values of applied potentials. For all potentials, the currents decrease exponentially as a function of the TEA concentration, as illustrated in Fig. 3. The inward currents obtained from BD simulations are reduced to 50% of the control value at the TEA concentrations of 19.0, 16.0, and 12.3 mM when the applied potentials are, respectively,  $-140$ ,  $-168$ , and  $-196$  mV (inside negative with respect to outside). Thus, the magnitude of attenuation of the inward current by TEA depends on its concentration as well as the applied potential. The inhibitory constants  $k_i$  we obtain at all applied potentials are higher than the experimentally-determined value, which is 3.2 mM at 200 mV [1].

Clearly, the well attracting TEA to the binding site needs to be deeper than that shown in Fig. 2C to account for the experimentally-determined affinity of extracellular TEA blockade. One possibility is that the aromatic residues move inward in the course of activation such that the radius of the pocket formed by them is reduced. We

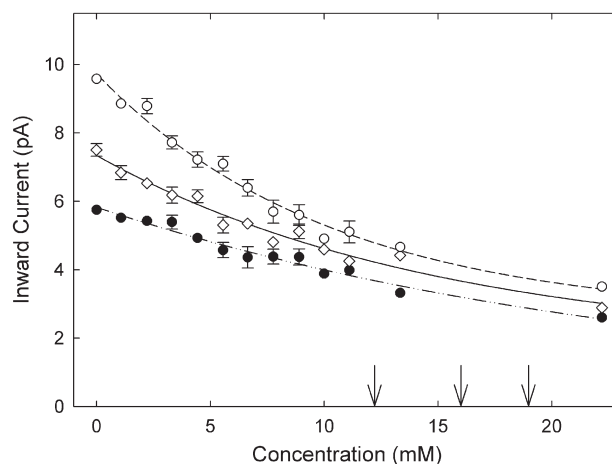


**Fig. 3.** Current-TEA-concentration curves. The current flowing across the channel at different TEA concentrations is determined under the applied potentials of  $-196$  mV (open circles),  $-168$  mV (open triangles), and  $-140$  mV (filled circles). The data points are fitted with exponential functions. The downward arrows indicate the calculated inhibitory constants  $k_i$  from the fitted curve. Error bars in this and all subsequent figures have a length of 2 S.E.M., and are not shown when they are smaller than the data points.

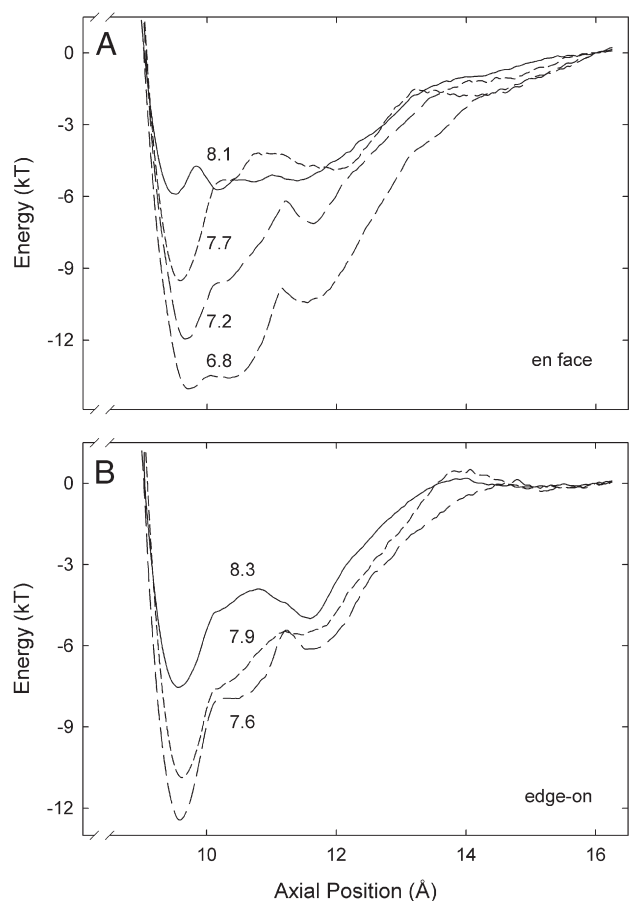


**Fig. 4.** Free energy profiles derived from various configurations of the aromatic rings of TYR82. (A) Four free energy profiles are constructed by positioning the aromatic rings of the tyrosine residues in an *en face* orientation. The radius of the binding cage, defined as the distance from the central axis of the pore and the carbon- $\gamma$  that is attached to the carbon- $\beta$  of TYR82, is reduced from 8.1 to 6.8 Å. (B) Three free energy profiles are constructed by positioning the aromatic rings in an edge-on configuration. The three profiles are obtained with the radius of the binding cage fixed at 8.3, 7.9, and then 7.6 Å.

check if the depth of the free energy profile systematically increases as the side-chains of the tyrosine residues are moved closer to each other. First, we position the aromatic rings in an *en face* orientation from the starting coordinates used for this study. This maneuver causes the radius to change from 8.3 Å to 8.1 Å. We then move the side-chains inward such that the radii they form become 7.7, 7.2 and 6.8 Å. Similarly, we reduce the radii of the binding pocket of the edge-on configuration step-wise from 8.3 to 7.9 and 7.6 Å. At each geometry of the aromatic residues, we construct, after an equilibration period of 200 ps, a set of 4 to 8 free energy profiles. The Boltzmann-averaged free energy profiles at 7 different radii formed by the side-chains of four tyrosine residues are illustrated in Fig. 4. In an *en face* configuration, as the radius decreases from 8.1 to 7.7, 7.2, and 6.8 Å, the depth of the free energy at  $z = 9.3$  Å increases from 5.8 to 9.5, 11.8, and 13.7 kT, respectively (Fig. 4A). Similarly, in an edge-on configuration, the depth of the free energy increases from 7.5 kT to 10.8 and 12.4 kT when the radius is decreased from 8.3 Å to 7.9 and 7.6 Å (Fig. 4B).

The *en face* free energy profile obtained with the radius of 7.7 Å, shown in Fig. 4A, is converted to a one-dimensional potential energy profile. The depth of the potential profile, once converted from the free energy profile, is 12.4 kT. After incorporating it to the BD algorithm, two current-TEA-concentration curves are obtained using an applied potential of -140 mV (Fig. 5A, filled circles) and -196 mV (open circles). The currents are reduced to 50% of the control values at TEA concentrations of 7.5 mM and 5.0 mM with the applied potentials

of -140 and -196 mV, respectively. The experimental  $k_i$  value, reported by Heginbotham et al. [1], is 3.2 mM at 200 mV, and their measured values are shown as open diamonds. Fig. 5B shows where in the channel  $K^+$  and TEA ions dwell preferentially during the conduction process. To obtain the dwell histogram, the channel is divided into 100 thin sections, and the number of ions in each slice is counted during a simulation period of 6.4  $\mu$ s. The concentration of TEA in the external reservoir during the simulation is 5.6 mM. There is a sharp peak centered at  $z = 24$  Å (dark bars), indicating that a TEA molecule, when it blocks the channel, stays at a fixed position just outside the selectivity filter. The distribution of  $K^+$  ions inside the channel, as expected, shows two main peaks in the selectivity filter and an additional peak near the intracellular entrance, created by four acidic residues, GLU118, guarding the gate (Fig. 5B).

In some  $K^+$  channels, such as the mutant *Shaker* T449Y, currents are halved in the presence of submillimolar TEA concentrations [6]. To ascertain how deep the free energy well needs to be to reproduce the  $k_i$  value derived from the mutant *Shaker*, we select the free energy profile obtained from the binding pocket radius of 7.2 Å and construct the current-TEA-concentration curve. The depths of the free energy

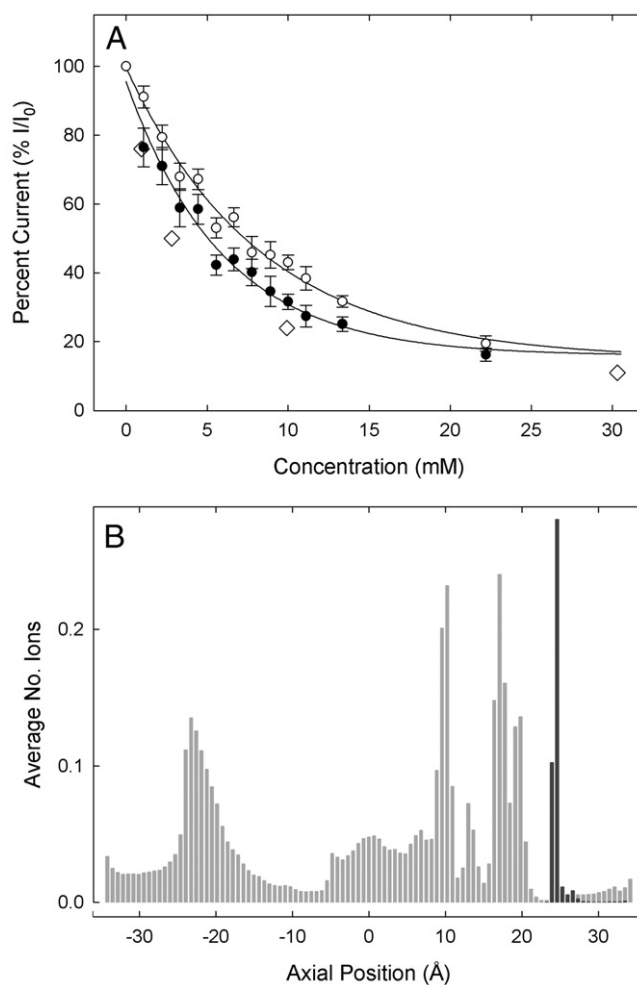


**Fig. 5.** Reduction of the currents by externally applied TEA and dwell histogram. The results of BD simulations are obtained with the profile derived with an *en face* orientation of the aromatic rings with the radius of 7.7 Å. (A) The attenuation of the currents by TEA is determined with the applied potentials of -196 mV (open circles) and -140 mV (filled circles). The currents at each TEA concentration are normalized to the control current. The inhibitory constants  $k_i$  derived from the two curves are 7.5 and 5.0 mM. The measurements obtained experimentally by Heginbotham et al. [1] are shown as open diamonds. (B) The channel is divided into 100 thin sections and the average number of  $K^+$  (light bars) and TEA (dark bars) in each section during the simulation period of 6.4  $\mu$ s is tabulated and plotted in the form of a histogram.

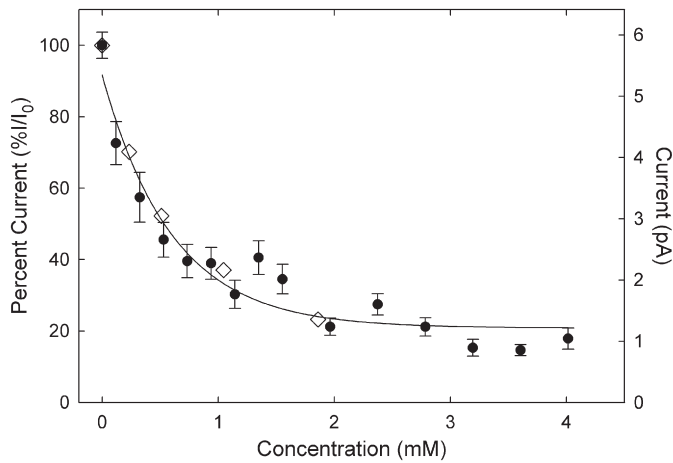


**Fig. 6.** The current-TEA-concentration curve obtained with a deep energy well. The free energy profile derived from the radius of 7.2 Å (shown in Fig. 4A) is used to determine the currents flowing across the channel under various TEA concentrations. Superimposed on the curve as open diamonds are the currents measured experimentally from the mutant *Shaker T449Y* by MacKinnon and Yellen [6].

well and potential energy well at  $z = 9.3$  Å are, respectively, 11.8 and 14.9 kT. The data plotted in Fig. 6 (filled circles) are obtained from symmetric 300 mM solutions in the reservoirs, with an applied potential of  $-196$  mV. Superimposed on the curve, indicated in open diamonds, are the experimental measurements obtained by MacK-

innon and Yellen [6]. The inhibitory constant we obtain from our simulated data is 0.58 mM, which closely matches the experimental value.

The results from BD simulations show that externally applied TEA binds to the binding pocket located just exterior to the selectivity filter and becomes unbound according to a first-order Markovian process. We first record the times at which a TEA molecule enters and then leaves the binding pocket during a simulation period of 19.2  $\mu$ s, with a TEA concentration of 5.6 mM and an applied potential of  $-196$  mV. The free energy profile used for this series of simulation is the one used to generate the previous figure (Fig. 5). We then tabulate the durations the binding pocket is occupied by a TEA molecule (on-time) and unoccupied (off-time). The results are presented in the form of interval histograms (Fig. 7). The interval histograms showing the on-time (Fig. 7A) and off-time (Fig. 7B) are distributed exponentially, indicating that the kinetics of binding and unbinding of TEA to the binding pocket is a first-order Markov process [44]. When a TEA molecule is in the binding pocket, the passage of  $K^+$  ions is effectively blocked.

The precise inhibitory constant  $k_i$  depends both on the concentration of KCl in the outer reservoir and the magnitude of the applied potential. We construct in Fig. 8A, using the free energy profile obtained with the radius of 7.7 Å, the current-KCl-concentration curves with (filled circles) and without TEA (open circles) in the external reservoir. Throughout, the TEA concentration and the applied potential are kept constant at 5.6 mM and  $-196$  mV, respectively. The

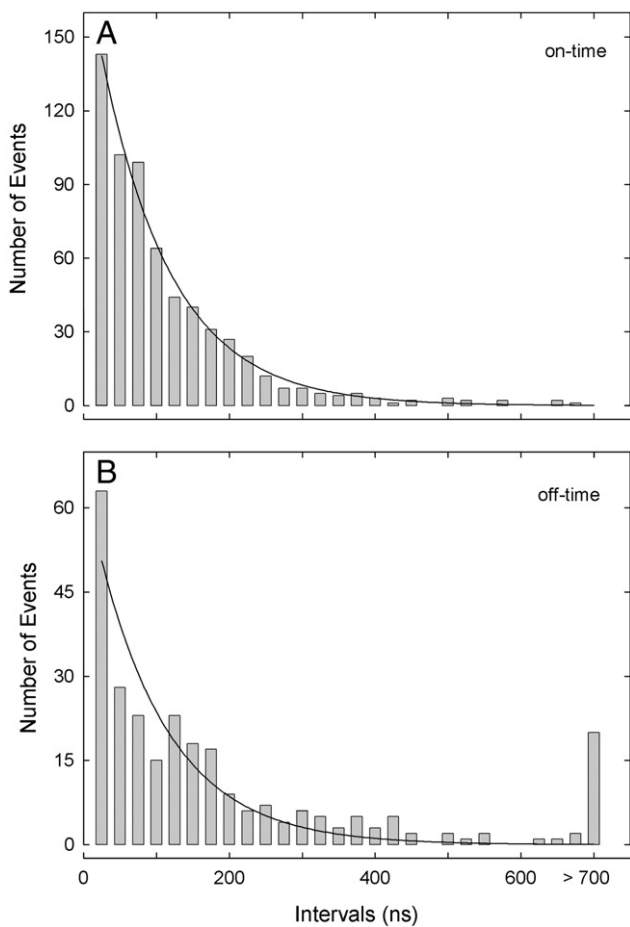


**Fig. 7.** Histograms of the durations the channel is blocked (A) and unblocked (B) by a TEA molecule in the binding cage. Successive time intervals during which the channel is occupied by TEA in the binding cage during the simulation period of 19.2  $\mu$ s are tabulated and the results are presented in the form of interval histograms. Exponential decay curves are fitted through the bar graphs (solid lines).

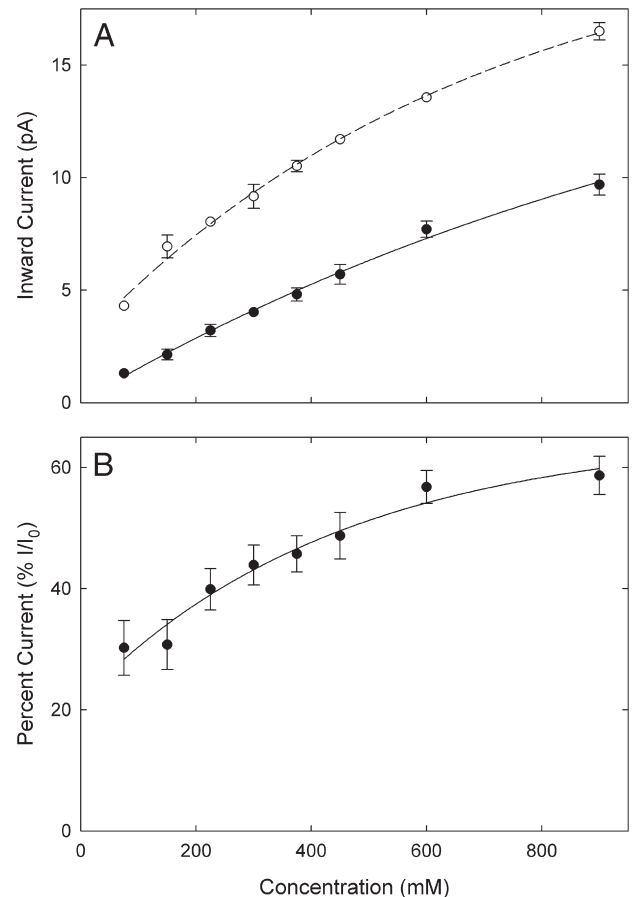


**Fig. 8.** Effectiveness of TEA blockade at different  $K^+$  concentrations. The potential profile used is the same as the one used previously to generate Fig. 5 (the radius of the binding cage is 7.7 Å). (A) The control conductance-concentration curve, shown as open circles, is obtained with an applied potential of  $-196$  mV with no TEA in the reservoir. Then, simulations are repeated, this time with a TEA concentration of 5.6 mM in the external reservoir (filled circles). (B) The percentage of the current relative to the control current is plotted as a function of the  $K^+$  concentration.

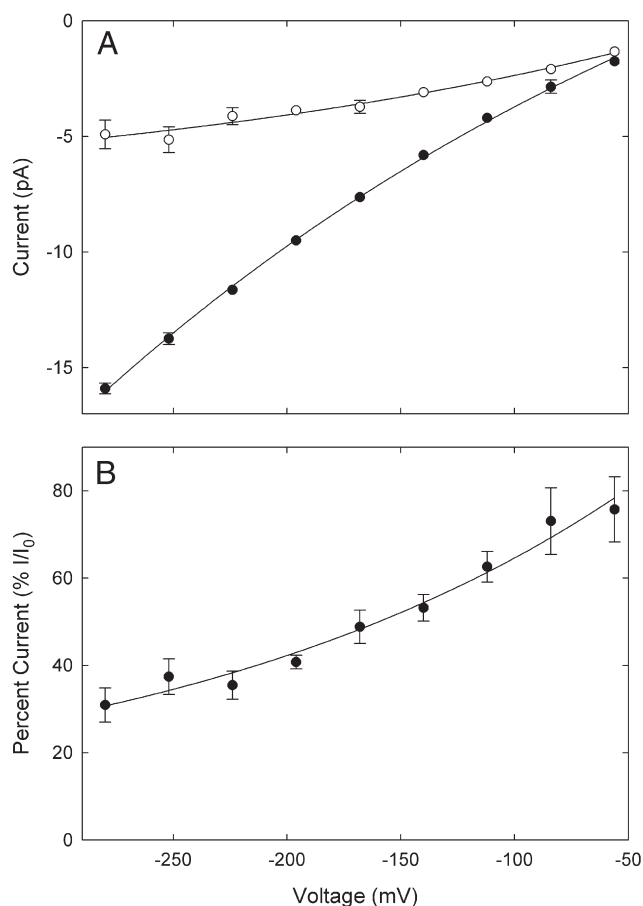


**Fig. 9.** Reduction of the currents at different applied potentials. The TEA concentrations in the external reservoir and the potential profile are the same as those used for Fig. 8. The concentration of K<sup>+</sup> ions in both reservoirs is kept constant at 300 mM. (A) The current increased monotonically with an increasing applied potential in the absence (filled circles) and presence (open circles) of TEA. (B) The percentage of the current relative to the control current decreases steadily as the applied potential is increased.

control under both conditions increases monotonically with an increasing ionic concentration. The percentage of attenuation caused by TEA of a fixed concentration decreases as the ionic concentration in the reservoirs is increased, as shown in Fig. 8B. For example, the current in the presence of 5.6 mM TEA in the external reservoir is reduced to 30% of the control value when the ionic concentration in the reservoir is 75 mM. The corresponding value at the KCl concentration of 900 mM is 57%.

We next explore how external TEA blockade is influenced by the applied potential. With a fixed TEA concentration of 5.6 mM TEA, and with the potential profile used for the previous series of simulations (Fig. 8), we determine the currents flowing across the channel at various applied potentials. The concentrations of K<sup>+</sup> ions in both reservoirs are kept constant at 300 mM. The inward current obtained with (open circles) and without TEA (filled circles) in the external reservoir is plotted against applied potentials in Fig. 9A. The currents under both conditions increase monotonically with the applied potentials. The percentage of currents attenuated by 5.6 mM TEA in the external vestibule, however, changes from 25% of the control current at the applied potential of -56 mV to 70% at -280 mV. Thus, for a fixed concentration, external TEA blockade becomes progressively more effective as the driving force is increased.

### 3.3. Structural observations

The crystal structure of KcsA reveals that the TYR82 side-chains rings assume an edge-on orientation [15], whereas an *en face*

orientation gives the optimal  $\pi$ -TEA interaction [7]. The question naturally arises: which of the two possible configurations of the aromatic rings is energetically more favorable? Here we show that edge-on is the lowest, stable energy configuration whether or not a TEA molecule is present in the binding site.

We carry out a series of runs beginning with the TYR82 rings in well-equilibrated *en face* orientations, and release the constraints that hold them *en face*. The starting coordinates are taken from runs that include over 1000 ps of simulation at radius 8.1 Å followed by 400 ps at radius 7.7 Å (see Fig. 4A). The *en face* constraints are replaced by backbone constraints very similar to those used previously (Fig. 4B). We find that, within 100 ps of further simulation, the TYR82 rings swing around to typical edge-on orientations, regardless of the position of the TEA molecule above its binding site.

Our BD results show that TEA binding becomes stronger as the radius of the binding cage is reduced (see Fig. 4). This observation holds whether the aromatic rings of the TYR82 are in an edge-on orientation or *en face* orientation. For detailed analyses, we generate the radial distribution function for hydrogens from water molecules relative to the carbonyl oxygens of the four TYR78 residues. First, we place the TEA at  $z = 11$  Å, which is 1.5 Å above the position where the energy well is the deepest. Using the rdfsol module in CHARMM, we then generate the radial distribution function for hydrogens from water molecules relative to the carbonyl oxygens of the four TYR78 residues. These oxygens form the top of the selectivity filter, and are in

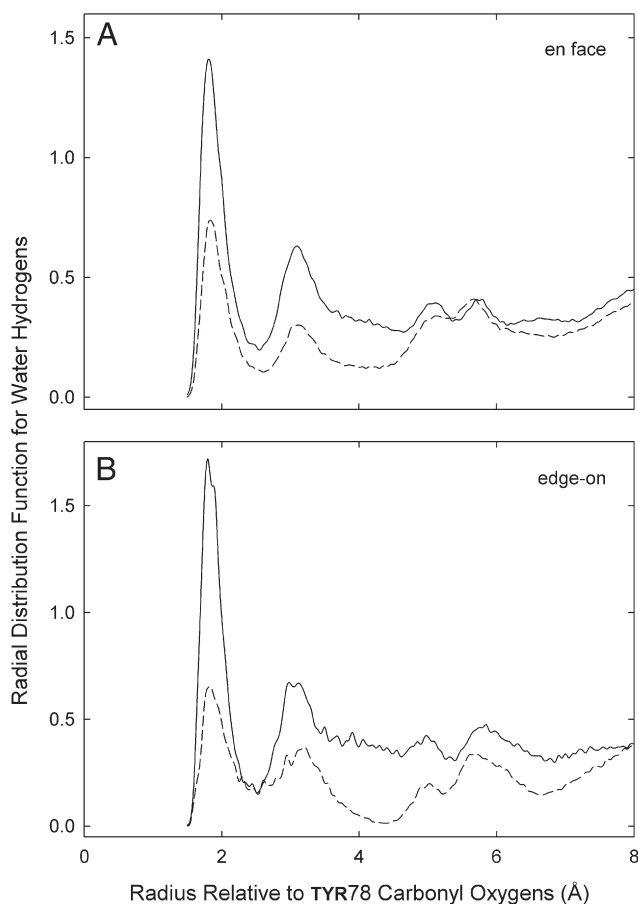


**Fig. 10.** The radial distribution functions for hydrogens from water molecules relative to the carbonyl oxygen of the four TYR78 residues. (A) The two curves are obtained with an *en face* orientation of the aromatic rings at two different radii of the binding cage. The upper curve (solid line) and lower curve (broken line) are derived with the radius of the binding cage fixed, respectively, at 8.1 Å and 7.2 Å. (B) The two curves are obtained with an *edge-on* orientation. The upper (solid line) and lower (broken line) curves are derived with the radius of the binding cage fixed, respectively, at 8.3 Å and 7.6 Å.

contact with the TEA molecule when it is sitting at the bottom of its binding site. The filter contains ions and water molecules in order W-K-W-K from the top downward, and these water molecules in the selectivity filter are also counted in the radial distributions. Any other water molecules within the first few angstroms must be contained in the gap between the TYR78 oxygens and the underside of the TEA molecule.

Fig. 10 shows the resulting radial distribution functions, each generated from 160 ps of data. The two sets of the graphs shown in Fig. 10A and B are obtained with, respectively, an *en face* orientation and an edge-on orientation of the aromatic rings. For each configuration, we compare the radial distribution functions obtained from two different radii of the binding cage: 7.2 Å vs. 8.1 Å for (A), and 7.6 Å vs. 8.3 Å for (B). The curves obtained with the larger of the two radii are shown in solid lines. The first peaks for all curves, whose maxima are at  $z = 1.8$  Å, correspond to water-hydrogens directly in contact with the TYR78 carbonyl oxygens, and include the water molecule inside the top of the selectivity filter. The comparison of two radial distribution functions (solid lines and broken lines) shows the pronounced effect of reducing the radius of the binding cage. At least half of the water molecules beneath and around the TEA are expelled. The gap between TEA and protein in some areas is only just big enough for a water molecule to fit. Thus, a small reduction of the radius of the binding cage causes an expulsion of water molecules that are normally present with a larger radius. This reduction of water molecules between the TEA and the selectivity filter produces a deeper attractive well as the radius of the binding cage is reduced slightly.

#### 4. Discussion

The shape of the TEA can best be approximated as an oblate spheroid whose long and short axes correspond to 2.3 Å and 4.6 Å. Thus, the molecules should ideally be represented and incorporated as asymmetrical rigid bodies and allowed both rotational and translational motions. For the present study, however, we approximate the shape of TEA as a sphere with a radius of 2.3 Å, deferring the more realistic representation of the molecule to a future study.

The attractive energy between TEA and the aromatic rings of the four tyrosine residues arises from the charge-quadrupolar moment and, possibly, the hydration forces [5,7–9]. Because in Brownian dynamics water molecules are not explicitly simulated, the interaction originating from the hydration force is not taken into account. Similarly, forces stemming from electrostatic interactions between a charged particle and quadrupolar moments are not calculated in the BD algorithm. We therefore implicitly account for these forces by incorporating in the BD algorithm a one-dimensional free energy profile obtained from molecular dynamics, so that each TEA molecule in the reservoir sees, in addition to all other attractive and repulsive forces it encounters, the attractive force generated by the tyrosine residues near the entrance of the selectivity filter. For use in BD, the profile of the potential of mean force derived from umbrella sampling calculations using weighted histogram analysis method [21] is converted into a potential energy profile, as described by Hoyles et al. [40]. An approach similar to the one we adopt here has been used previously [31,32,41]. In these studies, the one-dimensional electrostatic free energy of the ion in the gramicidin pore or the KcsA channel, derived from MD or otherwise, is incorporated in the BD algorithm to simulate the current flowing across the ion-conducting conduit.

Although we have exclusively used the PMF approach in deducing binding free energies of a TEA molecule with its binding cage, there are other microscopic methods that can be used for estimating these quantities. Luzhkov and Åqvist [9,42], for example, obtained the binding free energies of the quaternary ammonium ions with the KcsA channel using either the linear interaction energy method or the microscopic free energy perturbation approach. The problems

associated with each of these approaches are discussed by Warshel and his colleagues [31,32,43]. They point out that local errors in the PMF calculations can accumulate and cause global errors as an ion traverses a long, narrow channel. In our study, however, the use of the profile obtained from the PMF approach can readily be justified. The TEA can traverse only a short distance once it enters the pore; the height of the binding cage formed by four aromatic rings of the tyrosine residues extends only about 5 to 6 Å (see Fig. 2). Moreover, the PMF method allows all possible orientations of the TEA molecule at all points along the path.

In the novel algorithm we devised, the motion of TEA is influenced by the electrostatic, random, and frictional forces, as well as the attractive free energy profile derived from the PMF. This free energy profile, which is invisible to other charged particles in the simulation assembly, is in turn modulated by the locations of resident  $K^+$  ions in the selectivity filter. With these simulation techniques, we uncover several additional insights into the mechanisms of external TEA blockade. We determine the precise depth of the free energy profile external TEA has to encounter to reproduce the experimentally determined inhibitory constant (Figs. 5A and 6). When the depth of the free energy profile at the center of the binding pocket is  $-9.5$  kT, we obtain the inhibitory constant  $k_i$  of 5 mM, close to the experimental value obtained from the KcsA potassium channel [1]. When the depth of the potential profile is made deeper by 2 kT, the inhibitory constant is reduced to a submillimolar level, the value corresponding closely to that obtained from the T449Y *Shaker* potassium channel [6]. The depth of the profile, we demonstrate, is monotonically related to the radius of the binding cage. As the side-chains of the tyrosine residues are moved closer, the energy well encountered by TEA becomes deeper, regardless of whether the aromatic rings are in an edge-on configuration or an *en face* configuration. The small decrease in the radius of the binding cage has a pronounced effect on the hydration state of TEA as it approaches its blocking position near the selectivity filter.

The current across the KcsA channel decreases exponentially with an increasing TEA concentration. When a TEA molecule occupies the binding cage, the channel is effectively blocked. The probability of finding the channel being bound by a blocking molecule increases exponentially with its concentration. For any given ionic concentrations, the binding and unbinding of TEA to the binding cage obeys a first-order Markov process, governed by a  $2 \times 2$  stochastic transition matrix [44]. As a result, the interval histograms of the blocked and unblocked durations show exponential distributions (Fig. 7). Our detailed analyses of binding kinetics reveal that the time a molecule stays bound once it enters the binding cage depends primarily on the applied potential, whereas the time the channel remains open depends both on the TEA concentration in the reservoir and the applied potential [40]. Also, as the concentration of  $K^+$  ions in the external reservoir increases, the effectiveness of TEA blockade at a fixed concentration decreases. Thus, the affinity to external TEA block for a given depth of the free energy depends on the ionic concentration in the outer reservoirs (Fig. 8) and the applied potential (Fig. 9). An inhibitory constant  $k_i$  derived at a fixed potential with one ionic concentration does not hold true for different experimental conditions, as previous shown experimentally [45–49].

By grafting the free energy profiles obtained from MD onto the BD algorithm, we have been able to deduce many salient features of external TEA blockade in the KcsA  $K^+$  channel. Here we have exploited the capability of BD to measure the current flowing across a biological ion channel to elucidate the dynamic interaction taking place between the potassium channel and quaternary ammonium ions. We show how the free energy profile changes as the geometry of the aromatic ring forming the binding cage changes. The radius of the binding cage, but not the orientation of the aromatic side-chain of the tyrosine residues, has a pronounced effect on the depth of the

free energy well. By carrying out BD simulations in the KcsA potassium channels with TEA ions in KCl solutions, we show how the inward currents change with an increasing concentration of TEA in the simulation assembly. From a series of such current-concentration curves constructed from different energy profiles with varying well-depths, we are able to infer the depth of the energy well a TEA molecule needs to see to replicate the experimentally determined inhibitory constant for the TEA block. Moreover, by tabulating how long a TEA molecule stays bound in the binding site, we reveal the dynamics of binding and unbinding processes taking place in a fast time-scale. The technique we introduce here can be fruitfully utilized in examining other  $K^+$  channel models whose atomic coordinates are not yet determined. Any homology model of a  $K^+$  channel constructed must account for not only its current-voltage-concentration profiles, but also the effects of quaternary ammonium ions on channel currents.

### Acknowledgments

This work was supported by grants from the National Health & Medical Research Council of Australia. We thank Dan Gordon and Taira Vora for their helpful comments on the manuscripts.

### References

- [1] L. Heginbotham, M. LeMasurier, L. Kolmakova-Partensky, C. Miller, Single *Streptomyces lividans*  $K^+$  channels: functional asymmetries and sidedness of proton activation, *J. Gen. Physiol.* 114 (1999) 551–559.
- [2] S.R. Ikeda, S.J. Korn, Influence of permeating ions on potassium channel block by external tetraethylammonium, *J. Physiol.* 486 (1995) 267–272.
- [3] D. Immke, M.J. Wood, L. Kiss, S.J. Korn, Potassium-dependent changes in the conformation of the Kv2.1 potassium channel pore, *J. Gen. Physiol.* 113 (1999) 819–836.
- [4] D. Meuser, H. Splitt, R. Wagner, H. Schrepf, Exploring the open pore of the potassium channel from *Streptomyces lividans*, *FEBS Letts* 462 (1999) 447–452.
- [5] L. Heginbotham, L.R. MacKinnon, The aromatic binding site for tetraethylammonium ion on potassium channels, *Neuron* 8 (1998) 483–491.
- [6] R. MacKinnon, G. Yellen, Mutations affecting TEA blockade and ion permeation in voltage-activated  $K^+$  channels, *Science* 250 (1990) 276–279.
- [7] C.A. Ahern, A.L. Eastwood, H.A. Lester, D.A. Dougherty, R. Horn, A cation- $\pi$  interaction between extracellular TEA and an aromatic residue in potassium channels, *J. Gen. Physiol.* 128 (2006) 649–657.
- [8] S. Crouzy, S. Bernéche, B. Roux, Extracellular blockade of  $K^+$  channels by TEA: results from molecular dynamics simulations of the KcsA channel, *J. Gen. Physiol.* 118 (2001) 207–217.
- [9] V.B. Luzhkov, J. Åqvist, Mechanisms of tetraethylammonium ion block in the KcsA potassium channel, *FEBS Letts* 495 (2001) 191–196.
- [10] J. Consiglio, P. Andralib, S.J. Korn, Influence of pore residues on permeation properties in the Kv2.1 potassium channel. Evidence for a selective functional interaction of  $K^+$  with the outer vestibule, *J. Gen. Physiol.* 121 (2003) 111–124.
- [11] J. Consiglio, S.J. Korn, Influence of permeant ions on voltage sensor function in the Kv2.1 potassium channel, *J. Gen. Physiol.* 123 (2004) 387–400.
- [12] A. Cha, F. Bezanilla, Characterizing voltage-dependent conformational changes in the *Shaker*  $K^+$  channel with fluorescence, *Neuron* 19 (1997) 1127–1140.
- [13] G. Yellen, D. Sodickson, T.-Y. Chen, M.E. Jurman, An engineered cysteine in the external mouth of a  $K^+$  channel allows inactivation to be modulated by metal binding, *Biophys. J.* 66 (1994) 1068–1075.
- [14] L. Kiss, S.J. Korn, Modulation of C-type inactivation by  $K^+$  at the potassium channel selectivity filter, *Biophys. J.* 74 (1998) 1840–1849.
- [15] D.A. Doyle, J.M. Cabral, R.A. Pfuetzner, A. Kuo, J.M. Gulbis, S.L. Cohen, B.T. Chait, R. MacKinnon, The structure of the potassium channel: molecular basis of  $K^+$  conduction and selectivity, *Science* 280 (1998) 69–77.
- [16] S.H. Chung, T.W. Allen, S. Kuyucak, Conducting-state properties of the KcsA potassium channel from molecular and Brownian dynamics simulations, *Biophys. J.* 82 (2002) 628–645.
- [17] S.H. Chung, T.W. Allen, S. Kuyucak, Modeling diverse range of potassium channels with Brownian dynamics, *Biophys. J.* 83 (2002) 263–277.
- [18] B.R. Brooks, R.E. Bruccoleri, B.D. Olafson, D.J. States, S. Swaminathan, M. Karplus, CHARMM: A program for macromolecular energy, minimization, and dynamics calculations, *J. Comp. Chem.* 4 (1983) 183–217.
- [19] A.D.J. MacKerell, D. Bashford, R.L. Dunbrack, J.D. Evanseck, M.J. Fields, S. Fischer, J. Gao, H. Guo, D.J.-M. S. Ha, et al., All-atom empirical potential for molecular modeling and dynamics studies of proteins, *J. Phys. Chem. B* 102 (1998) 3586–3616.
- [20] G.M. Torrie, J.P. Valleau, Nonphysical sampling distributions in Monte Carlo free-energy estimation—Umbrella sampling, *J. Comp. Phys.* 23 (1997) 187–199.
- [21] S. Kumar, D. Bouzida, R.H. Swendsen, P.A. Kollman, J.M. Rosenberg, The weighted histogram analysis method for free-energy calculations on biomolecules: 1. The method, *J. Comp. Chem.* 13 (1992) 1011–1021.
- [22] S.C. Li, M. Hoyles, S. Kuyucak, S.H. Chung, Brownian dynamics study of ion transport in the vestibule of membrane channels, *Biophys. J.* 74 (1998) 37–47.
- [23] M. Hoyles, S. Kuyucak, S.H. Chung, Computer simulation of ion conductance in membrane channels, *Phys. Rev. E* 58 (1998) 3654–3661.
- [24] S.H. Chung, T. Allen, M. Hoyles, S. Kuyucak, Permeation of ions across the potassium channels: Brownian dynamics studies, *Biophys. J.* 77 (1999) 2517–2533.
- [25] M. Hoyles, S. Kuyucak, S.H. Chung, Solutions of Poisson's equation in channel-like geometries, *Comput. Phys. Comm.* 115 (1998) 45–68.
- [26] L. Pauling, *The Nature of the Chemical Bond*, Cornell University Press, Ithaca, N.Y., 1942.
- [27] M. Hoyles, S. Kuyucak, S.H. Chung, Energy barrier presented to ions by the vestibule of the biological membrane channel, *Biophys. J.* 70 (1996) 1628–1642.
- [28] C. Schultz, A. Warshel, What are the dielectric 'constant' of proteins and how to validate electrostatic models? *Proteins* 44 (2001) 400–417.
- [29] P.E. Smith, R.M. Brunne, A.E. Mark, W.F. van Gunsteren, Dielectric properties of trypsin inhibitor and lysozyme calculated from molecular dynamics simulations, *J. Phys. Chem.* 97 (1993) 2009–2014.
- [30] T. Simonson, C.L. Brooks III, Charge screening and the dielectric constant of proteins: insights from molecular dynamics, *J. Am. Chem. Soc.* 118 (1996) 8452–8458.
- [31] A. Burykin, C.N. Schutz, J. Villa, A. Warshel, Simulations of ion current in realistic models of ion channels: the KcsA potassium channel, *Proteins* 47 (2002) 265–280.
- [32] A. Burykin, M. Kato, A. Warshel, Exploring the origin of the ion selectivity of the KcsA potassium channel, *Protein* 52 (2003) 412–426.
- [33] G. King, F.S. Lee, A. Warshel, Microscopic simulations of macroscopic dielectric constants of solvated proteins, *J. Chem. Phys.* 95 (1991) 4366–4377.
- [34] J.A. Ng, T. Vora, V. Krishnamurthy, S.H. Chung, Estimating the dielectric constant of the channel protein and pore, *Eur. Biophys. J.* 37 (2007) 213–222.
- [35] W. Im, S. Seefeld, B. Roux, A grand canonical Monte Carlo-Brownian dynamics algorithm for simulating ion channels, *Biophys. J.* 79 (2000) 788–801.
- [36] B. Corry, B.M. Hoyles, T.W. Allen, M. Walker, S. Kuyucak, S.H. Chung, Reservoir boundaries in Brownian dynamics simulations of ion channels, *Biophys. J.* 82 (2002) 1975–1984.
- [37] T.W. Allen, S. Kuyucak, S.H. Chung, Molecular dynamics estimates of ion diffusion in model hydrophobic and KcsA potassium channels, *Biophys. Chem.* 86 (2000) 1–14.
- [38] B. Hille, *Ion Channels of Excitable Membranes*, Sinauer Associates, Inc., Sunderland, MA, 2001.
- [39] W.H. Press, B.P. Flannery, S.A. Teukolsky, W.T. Vetterling, *Numerical Recipes*, Cambridge University Press, New York, 1993.
- [40] M. Hoyles, V. Krishnamurthy, M. Siksik, S.H. Chung, Brownian dynamics theory for predicting internal and external blockages of tetraethylammonium ion the KcsA potassium channel, *Biophys. J.* 94 (2008) 366–378.
- [41] S. Edwards, B. Corry, S. Kuyucak, S.H. Chung, Continuum electrostatics fails to describe ion permeation in the gramicidin channel, *Biophys. J.* 83 (2002) 1348–1360.
- [42] V.B. Luzhkov, F. Österberg, J. Åqvist, Structure-activity relationship for extracellular block of  $K^+$  channels by tetraalkylammonium ions, *FEBS Letts* 554 (2003) 159–164.
- [43] M. Kato, A. Warshel, Through the channel and around the channel: validating and comparing microscopic approaches for the evaluation of free energy profiles for ion permeation through ion channels, *J. Phys. Chem. B.* 109 (2005) 19516–19522.
- [44] S.H. Chung, J.B. Moore, L. Xia, L.S. Premkurmar, P.W. Gage, Characterization of single channel currents using digital signal processing techniques based on hidden Markov models, *Phil. Trans. R. Soc. Lond. B* 329 (1990) 256–285.
- [45] D. Oliver, H. Hahn, C. Antz, J.P. Ruppersberg, B. Fakler, Interaction of permeant and blocking ions in cloned inward-rectifier  $K^+$  channels, *Biophys. J.* 74 (1998) 2318–2326.
- [46] M. Spassova, Z. Lu, Coupled ion movement underlies rectification in an inward-rectifier  $K^+$  channel, *J. Gen. Physiol.* 112 (1998) 211–221.
- [47] M. Spassova, Z. Lu, Tuning the voltage dependence of tetraethylammonium block with permeant ions in an inward-rectifier  $K^+$  channel, *J. Gen. Physiol.* 114 (1999) 415–426.
- [48] J. Thompson, T. Begenisich, External TEA block of *Shaker*  $K^+$  channel is coupled to the movement of  $K^+$  ions within the selectivity filter, *J. Gen. Physiol.* 122 (2003) 239–246.
- [49] E. Kutluay, B. Roux, L. Heginbotham, Rapid intracellular TEA block of the KcsA potassium channel, *Biophys. J.* 88 (2005) 1018–1029.